AC biochemistry

DATASET · JUNE 2014

READS
32

11 AUTHORS, INCLUDING:

Arundhati Chattopadhyay
The Methodist Hospital System
3 PUBLICATIONS **32** CITATIONS
SEE PROFILE

Barbara Campanini
Università degli studi di Parma
56 PUBLICATIONS **770** CITATIONS
SEE PROFILE

Stefano Bettati
Università degli studi di Parma
96 PUBLICATIONS **1,991** CITATIONS
SEE PROFILE

Andrea Mozzarelli
Università degli studi di Parma
215 PUBLICATIONS **5,022** CITATIONS
SEE PROFILE

Structure, Mechanism, and Conformational Dynamics of *O*-Acetylserine Sulfhydrylase from *Salmonella typhimurium*: Comparison of A and B Isozymes†

Arundhati Chattopadhyay,‡,§ Markus Meier,§ Sergei Ivaninskii,|| and Peter Burkhard*,§

Institute of Materials Science, University of Connecticut, 97 North Eagleville Road, Storrs, Connecticut 06269-3136, and M. E. Müller Institute for Structural Biology, Biozentrum, University of Basel, 4056 Basel, Switzerland

Francesca Speroni,‡ Barbara Campanini,* Stefano Bettati, and Andrea Mozzarelli

Department of Biochemistry and Molecular Biology, University of Parma, 43100 Parma, Italy

Wael M. Rabeh,‡ Lei Li,⊥ and Paul F. Cook*

Department of Chemistry and Biochemistry, University of Oklahoma, 620 Parrington Oval, Norman, Oklahoma 73019

Received December 19, 2006; Revised Manuscript Received April 2, 2007

ABSTRACT: *O*-Acetylserine sulfhydrylase is a pyridoxal 5′-phosphate-dependent enzyme that catalyzes the final step in the cysteine biosynthetic pathway in enteric bacteria and plants, the replacement of the β-acetoxy group of *O*-acetyl-L-serine by a thiol to give L-cysteine. Two isozymes are found in *Salmonella typhimurium*, with the A-isozyme expressed under aerobic and the B-isozyme expressed under anaerobic conditions. The structure of *O*-acetylserine sulfhydrylase B has been solved to 2.3 Å and exhibits overall a fold very similar to that of the A-isozyme. The main difference between the two isozymes is the more hydrophilic active site of the B-isozyme with two ionizable residues, C280 and D281, replacing the neutral residues S300 and P299, respectively, in the A-isozyme. D281 is above the *re* face of the cofactor and is within hydrogen-bonding distance to Y286, while C280 is located about 3.4 Å from the pyridine nitrogen (N1) of the internal Schiff base. The B-isozyme has a turnover number (V/E_t) 12.5-fold higher than the A-isozyme and an ∼10-fold lower K_m for *O*-acetyl-L-serine. Studies of the first half-reaction by rapid-scanning stopped-flow indicate a first-order conversion of the internal Schiff base to the α-aminoacrylate intermediate at any concentration of *O*-acetyl-L-serine. The K_d values for formation of the external Schiff base with cysteine and serine, obtained by spectral titration, are pH dependent and exhibit a pK_a of 7.0−7.5 (for a group that must be unprotonated for optimum binding) with values, above pH 8.0, of about 3.0 and 30.0 mM, respectively. In both cases the neutral enolimine is favored at high pH. Failure to observe the pK_a for the α-amines of cysteine and serine in the pK_{ESB} vs pH profile suggests a compensatory effect resulting from titration of a group on the enzyme with a pK_a in the vicinity of the α-amine's pK_a. The pH dependence of the first-order rate constant for decay of the α-aminoacrylate intermediate to give pyruvate and ammonia gives a pK_a of about 9 for the active site lysine (K41), a pH unit higher than that of the A-isozyme. The difference in pH dependence of the pK_{ESB} for cysteine and serine, the higher pK_a for K41, and the preference for the neutral species at high pH compared to the A-isozyme can be explained by titration of C280 to give the thiolate. Subtle conformational differences between *O*-acetylserine sulfhydrylase A and *O*-acetylserine sulfhydrylase B are detected by comparing the absorption and emission spectra of the internal aldimine in the absence and presence of the product acetate and of the external aldimine with L-serine. The two isozymes show a different equilibrium distribution of the enolimine and ketoenamine tautomers, likely as a result of a more polar active site for *O*-acetylserine sulfhydrylase B. The distribution of cofactor tautomers is dramatically affected by the ligation state of the enzyme. In the presence of acetate, which occupies the α-carboxylate subsite, the equilibrium between tautomers is shifted toward the ketoenamine tautomer, as a result of a conformational change affecting the structure of the active site. This finding, in agreement with structural data, suggests for the *O*-acetylserine sulfhydrylase B-isozyme a higher degree of conformational flexibility linked to catalysis.

O-Acetylserine sulfhydrylase (OASS)[1] catalyzes the final reaction of the cysteine biosynthetic pathway in bacteria and plants, the conversion of *O*-acetyl-L-serine (OAS) and bisulfide to L-cysteine and acetate (*1*). In enteric bacteria there are two isozymes of OASS, A and B. The B-isozyme of *O*-acetylserine sulfhydrylase (OASS-B) is expressed in

† This work was supported by the Grayce B. Kerr endowment to the University of Oklahoma to support the research of P.F.C., the Swiss National Science Foundation and the M. E. Mueller Foundation (to P.B.), and grants from the Italian Ministry of University and Research (COFIN2005 to A.M.) and the International Exchange Program 2005 (to A.M. and P.F.C.). The Istituto Nazionale di Biostrutture e Biosistemi is gratefully acknowledged.

* Corresponding authors. P.F.C.: tel, 405-325-4581; fax, 405-325-7182; e-mail, pcook@ou.edu. P.B.: tel, 860-486-3830; fax, 860-486-4745; e-mail, Peter.Burkhard@uconn.edu. B.C.: tel, 39-0521906613; fax, 39-0521905151; e-mail, barbara.campanini@unipr.it.

‡ These authors contributed equally to the work.

§ University of Connecticut.

|| University of Basel.

⊥ Current address: Department of Biochemistry, Albert Einstein College of Medicine, 1300 Morris Park Ave., Bronx, NY 10461-1602.

10.1021/bi602603c CCC: $37.00
Published on Web 06/21/2007

Salmonella typhimurium under anaerobic growth conditions, and it appears to be less substrate selective than the A-isozyme for both the amino acid and nucleophilic substrates (*2*). OASS-B has a ping-pong kinetic mechanism on the basis of initial velocity studies obtained in the absence of inhibitors (*2*). The OASS-B reaction substitutes the acetoxy group of OAS with a thiol group to yield cysteine in a β-substitution reaction. The B-isozyme has a proposed chemical mechanism that is similar to that observed for the A-isozyme (*3*). The substrate, OAS, binds with its α-amine unprotonated to carry out a nucleophilic attack on C4′ of the internal Schiff base (ISB) to generate the OAS external Schiff base (ESB). The Schiff base lysine, which was in internal Schiff base linkage, acts as a general base to deprotonate C_α in the β-elimination reaction responsible for the release of acetate ending the first half-reaction.

Three-dimensional structures of the A-isozyme from *S. typhimurium* have been solved in the absence of ligands as an open form (*4*). A structure of the K41A mutant enzyme, isolated as a closed form with methionine bound to the active site pyridoxal 5′-phosphate (PLP) in external Schiff base linkage, has also been solved (*5*), as has the structure with chloride bound to an allosteric site at the dimer interface (*6*). These structures have been invaluable in deducing a number of aspects of the mechanism of the enzyme. Recently, a structure of the B-isozyme from *Escherichia coli* has also been solved (*7*), but fewer studies of this isozyme have been carried out to date.

The coenzyme PLP provides a valuable probe to protein dynamics and catalysis for PLP-dependent enzymes, due to its localization at the enzyme active site and the correlation of enzyme conformational changes with catalytic intermediates along the reaction pathway. Given this tight link between electronic and conformational states, it is not surprising that spectroscopic methods have been exploited to reveal the conformational landscape of catalytic action, including the open-to-closed transitions that occur in the conversion of the ISB to the ESB or other catalytic intermediates, such as quinonoid species or α-aminoacrylate (AA) Schiff bases (*8*−*12*). In these studies complex fluorescence emission properties were observed originating from changes in the ground and excited state equilibrium distribution between the enolimine and ketoenamine tautomers of catalytic intermediates (Scheme 1). Since this tautomeric equilibrium is strongly influenced by the polarity of the active site, with the enolimine being favored by a less polar environment (*13*), spectroscopic signals are sensitive to small differences in the polarity of the microenvironment where PLP is located. For OASS-A, previous investigations, reporting structured fluorescence emission and excitation spectra, indicated the occurrence of an enolimine-to-ketoenamine isomerization in the excited state (*10*).

Scheme 1: Tautomeric Equilibria for the Internal Schiff Base (ISB) the External Schiff Base (ESB) with Amino Acids, and α-Aminoacrylate (AA)

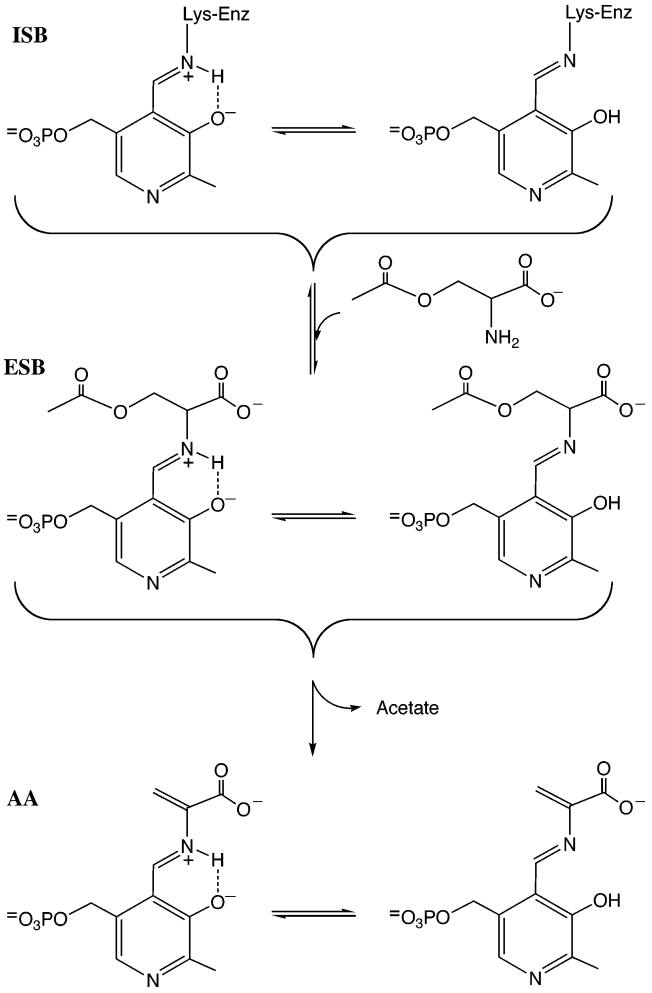

Previously, only small amounts of the B-isozyme could be purified (*2*, *3*), and limited spectral and kinetic studies could be carried out. We have recently overexpressed and purified OASS-B from *S. typhimurium* as the N-terminal His-tagged enzyme. In this paper, we report the X-ray crystal structure of OASS-B from *S. typhimurium*. In addition, in order to explain functional properties of OASS-B on the basis of its three-dimensional structure and to understand differences in structure−function relationships between OASS-A and OASS-B, kinetic and spectral studies are presented to mechanistically and conformationally characterize the B-isozyme.

MATERIALS AND METHODS

Chemicals. *O*-Acetyl-L-serine, DTNB, L-cysteine, and chloramphenicol were obtained from Sigma. The buffers Ches, Hepes, Mes, Taps, and imidazole were obtained from Research Organics. Ampicillin was obtained from Midwest Scientific. IPTG was obtained from Research Products International, and L-serine was obtained from Aldrich. Platinum *Pfx* DNA polymerase was from Invitrogen. The Ni-NTA resin was from Qiagen. All other chemicals and reagents were obtained from commercial sources and were of the highest purity available.

Enzyme Preparation. Recombinant OASS-A from *S. typhimurium* was expressed and purified following the

[1] Abbreviations: AA, α-aminoacrylate external Schiff base; ISB, internal Schiff base; ESB, external Schiff base; DTNB, 5,5′-dithiobis-(2-nitrobenzoate); DTT, dithiothreitol; IPTG, isopropyl β-thio-D-galactoside; OAS, *O*-acetyl-L-serine; OASS-A, A-isozyme of *O*-acetylserine sulfhydrylase; OASS-B, B-isozyme of *O*-acetylserine sulfhydrylase; PLP, pyridoxal 5′-phosphate; RSSF, rapid-scanning stopped-flow; TNB, 5-thio-2-nitrobenzoate; Ches, 2-(*N*-cyclohexylamino)ethanesulfonic acid; Hepes, *N*-(2-hydroxyethyl)piperazine-*N*′-2-ethanesulfonic acid; Mes, 2-(*N*-morpholino)ethanesulfonic acid; Taps, 3-[[tris(hydroxymethyl)]amino]propanesulfonic acid.

protocol previously described (*14*). Recombinant OASS-B from *S. typhimurium* was previously purified by the method of Tai et al. (*2*). In order to simplify the purification procedure, a 10-His tag was added at the amino terminus of the enzyme. The OASS-B gene, *cys*M, was subcloned into the pET16b vector by PCR amplification using the pRSM17 vector (*15*), which contains the *cys*M gene of *S. typhimurium* LT-2. Conditions for PCR cycling were as follows: denaturation at 94 °C for 40 s, primer annealing at 45 °C for 45 s, and primer elongation at 68 °C for 90 s. The cycle was repeated 35 times, and the reaction at the final stage was incubated for 10 min at 68 °C to complete any immature products. The PCR reaction was performed with platinum *Pfx* DNA polymerase. The primers used in the PCR have upstream *Nde*I and downstream *Xho*I restriction sites. The primer sequences are as follows with the bold letters representing the restriction site: forward primer, 5′-GGCTTTTTTACGAGCTGAA**CATATG**AATA-CATTAGAAC-3′; reverse primer, 5′-GGCCG**CTCGAG**CG-GTTAAATCCCTGCCCCCTGG-3′.

The new plasmid, WR-OASSB, adds a 10-His tag to the N-terminus of OASS-B together with a linker of 9 amino acids derived from the pET16b vector. The new vector was transformed into the BL21*(DE3)-RIL *E. coli* strain, which utilizes a T7 promoter-based expression system. The *E. coli* strain contains the RIL plasmid (pACYS) that confers chloramphenicol resistance and contains genes for rare tRNAs. Overnight cultures were inoculated in flasks containing LB medium, 50 μg/mL ampicillin, and 35 μg/mL chloramphenicol and grown at 30 °C. When the culture reached an OD_{600} of 0.7−0.9, it was induced by the addition of 0.5 mM IPTG and allowed to grow for 5 h. The pH was maintained at 7.0 during growth using 10 N KOH and 5 N HCl as needed. After centrifugation at 8000*g* for 30 min, the cell pellet was resuspended in 50 mM potassium phosphate and 300 mM NaCl, pH 7.8. Cells were sonicated for 3 min (1 min pulse followed by 30 s rest). After centrifugation, PLP (0.05 g/L) was added to the supernatant, and it was then stirred for 1 h at 4 °C. The solution was loaded onto a Ni-NTA agarose affinity column preequilibrated with 50 mM phosphate buffer and 300 mM NaCl, pH 7.8, and the column was washed with 10 volumes of 50 mM imidazole. The chromatogram was then developed in steps of 50 mM imidazole using 10 bed volumes. OASS-B eluted between 0.15 and 0.2 M imidazole. The enzyme-containing fraction was then dialyzed against 5 mM Hepes, pH 8.0, at 4 °C and stored at 4 °C. The A-isozyme was stored in 10 mM Hepes at −80 °C. On the basis of SDS−PAGE analysis both isozymes were >98% pure. The concentration of OASS-A protomers was calculated on the basis of the extinction coefficient at 412 nm of 7600 M^{-1} cm^{-1} (*16*). The extinction coefficient of OASS-B at 414 nm, 11500 M^{-1} cm^{-1}, was calculated from the amount of PLP released upon alkaline-induced denaturation of the protein fully saturated with PLP (*17*). Since chloride ion is known to be an inhibitor of both OASS-A and OASS-B activity (*2*), protein stock solutions were diluted or dialyzed against chloride-free buffer solutions prior to use.

Crystallization and Data Collection. Crystallization was performed by the hanging-drop vapor diffusion method at 295 K using 24-well tissue culture plates. Each hanging drop, prepared by mixing 2 μL of reservoir solution and 2 μL of protein solution (23 mg/mL, 5 mM Hepes, pH 8.0), was equilibrated against 1 mL of reservoir solution. Initial crystallization conditions were tested using the Hampton and Wizard crystal screen kits (Emerald Structures). Hexagonal rod-shaped crystals were grown using sodium−potassium tartrate as the precipitant. Crystals suitable for diffraction experiments were obtained from a protein solution mixed with 1 M sodium−potassium tartrate and 100 mM Mes, pH 6.0. The crystals were transferred through a series of cryoprotectant solutions of increasing glycerol concentration (5%, 10%, and 20%) before being flash-frozen in a cold nitrogen stream. X-ray diffraction data were collected at 100 K on a MarResearch detector at the Swiss Light Source (SLS), Villigen, Switzerland. The wavelength of the synchrotron radiation was 0.95109 Å. The data were processed and integrated using DENZO and scaled using SCALEPACK from the HKL program suite (*18*). The data processing statistics are shown in Table 1.

Table 1: Data Collection and Refinement Statistics

data collection statistics	
space group	*P*1
cell dimensions	
a, *b*, *c* (Å)	103.052, 106.948, 112.107
α, β, γ (deg)	95.59, 90.06, 117.61
resolution (Å)	50−2.3
$I/\sigma(I)$	5
completeness (%)	96.2
redundancy	2.9
refinement statistics	
no. of reflections	179465
R, R_{free} (%)	21.3, 23.7
no. of atoms	18444
protein	17696
PLP	120
water	628
average *B*-factors (Å^2)	
Wilson plot	42.8
protein	47.0
PLP	35.6
water	44.9
rms deviations from ideal	
bond lengths (Å)	0.012
bond angles (deg)	1.58

Structure Determination and Refinement. The calculated Matthew's coefficient (V_M) indicated the presence of 8−16 monomers in the asymmetric unit for data of 2.3 Å resolution (*19*). The actual number of chains turned out to be eight, which corresponds to a solvent content of 70% and a V_M of 4.17. The structure was solved by molecular replacement with the coordinates of the wild-type OASS-A enzyme [PDB code 1OAS (*4*)] as a search model. OASS-A has 43% sequence identity and was the most closely related structure available during data processing. The molecular replacement calculations using the program AMoRe (*20*) were performed with one monomer of the structure of OASS-A as a search model in space group *P*1. The atomic model was built using the program O (*21*), and the orientations and positions of the eight different monomers were determined. After rigid-body refinement, simulated annealing refinement and a density modification cycle were performed using CNS (*22*). The NCS restraints between all eight monomers were used at early stages of refinement. After manual building of all visible loops, the restraints were removed, and all the monomers were refined using CNS. Intricate NCS restraints between groups of side chains with similar orientations were

reintroduced at a late stage of refinement. These restraints dramatically decreased the R and R_{free} values. Weighted $2F_o - F_c$ and $F_o - F_c$ electron density maps were computed using CNS, and manual rebuilding of the model was done with the program O.

Calculation of Temperature Factors. The coordinates of the structures with entry codes 2BHT, 2BHS, 1OAS, 1FCJ, and 1D6S were retrieved from the RCSB protein database. Calculation of the average *B*-factors per protein was carried out with the program Baverage from the CCP4 suite (*23*). The average *B*-factor per residue, V_M, and the solvent content were calculated using the program CNS (*22*).

Enzyme Assay. OASS-B activity was monitored using TNB as a substrate analogue of bisulfide (*2*). The TNB was prepared fresh daily by the reduction of DTNB with the disulfide reducing agent DTT. The disappearance of TNB was monitored continually at 412 nm (ϵ_{412}, 13600 M^{-1} cm^{-1}) using a Beckman DU 640 spectrophotometer. All assays were performed in 100 mM Hepes, pH 7.0, at 25 °C.

Ultraviolet−Visible Spectral Studies. The absorbance spectra of OASS-B in the absence and presence of different concentrations of L-serine or L-cysteine were obtained as described previously for OASS-A (*24*). Amino acid substrates were added in a stepwise manner giving final concentrations of L-serine between 10 and 200 mM and L-cysteine between 1 and 100 mM. The pH was varied from 5.5 to 11.0 utilizing the following buffers at 100 mM final concentration: Mes, 5.5−6.5; Hepes, 6.5−8.0; Taps, 8.0−9.5; Ches, 9.5−11.0. Absorption spectra were measured at zero substrate concentration and after each substrate addition. To find λ_{max} for the reaction, a difference spectrum between the ESB at saturating cysteine (or serine) and the ISB in the absence of amino acid was obtained, giving a maximum absorbance change at 457 nm. All spectra were corrected for dilution and changes in the baseline absorbance (using the difference in absorbance at 550 nm). The ΔA_{457} was plotted vs the amino acid concentration to generate an estimate of K_{ESB}. A plot of pK_{ESB} vs pH was fitted to eq 3 (see below) to obtain the pK_a values of the group(s) on the substrate or enzyme involved in formation of the ESB form of the enzyme.

OAS:Acetate Lyase Activity. The first-order rate of degradation of the (AA) into pyruvate and ammonia was measured utilizing a Hewlett-Packard 8452A photodiode array spectrophotometer as described previously (*25*). OASS-B, maintained at a final concentration of 20 μM, was converted to the AA by adding a concentration of OAS ≤ OASS-B. The first-order rate constant for disappearance of AA was calculated, monitoring the absorbance at 472 and 327 nm, and the rate constant for the appearance of free enzyme was calculated, monitoring the absorbance at 414 nm. A fit of the data to a first-order rate law gave the first-order rate constant (k_{obs}). All rate constants were identical within experimental error. The experiment was carried out over the pH range 6.5−9.8 utilizing 200 mM buffer, as described above. A plot of log k_{obs} vs pH provided an estimate of the pK_a of the group involved in the lyase activity.

Initial Velocity and pH Studies. Initial velocity data were obtained as a function of one reactant at several fixed concentrations of the second reactant. The reactant concentrations were varied around their respective K_m values.

Rapid-Scanning Stopped-Flow Studies. Pre-steady-state kinetic measurements were carried out using an OLIS-RSM 1000 stopped-flow spectrophotometer. Sample solutions were prepared in two syringes at the same pH with a final buffer concentration of 200 mM; the pH was varied from 5.5 to 7.5 utilizing the buffers listed above. The first syringe contained OASS-B at a concentration no lower than 20 μM, while the second syringe contained different concentrations of OAS at final concentrations ranging from 0.1 to 10 mM, L-serine at final concentrations of 10−200 mM, or L-cysteine at final concentrations of 5−100 mM. Data were collected with a repetitive scan rate of 15 ms from 280 to 600 nm, and the number of scans collected depended on the rate of the reaction. The disappearance of the ISB was monitored at 414 nm, and the appearance of the AA was monitored at 472 and 327 nm. The rate data were fitted to eq 5 (see below) to obtain the first-order rate constant (k_{obs}), which was plotted vs substrate concentration and fitted to a linear equation to obtain the second-order rate constant (k_{max}/K_{ESB}). The log k_{max}/K_{ESB} was plotted vs pH to assess data quality and then fit to eq 3 to estimate the pK_a of the titrated group (see below).

Data Processing. Data were fitted to the appropriate rate equation using the Marquardt−Levenberg algorithm supplied with the EnzFitter program from BIOSOFT, Cambridge, U.K. Initial rate data were fitted to eq 1, which describes a ping-pong kinetic mechanism. The K_{ESB} values for cysteine and serine were obtained using the equation for a rectangular hyperbola (eq 2).

$$v = \frac{VAB}{K_aB + K_bA + AB} \tag{1}$$

$$\Delta A_{457}^{obs} = \frac{(\Delta A_{457}^{max})L}{K_{ESB} + L} \tag{2}$$

In eq 1, v and V are initial and maximum rates, respectively, A and B are reactant concentrations, while K_a and K_b are K_m values for A and B, respectively. In eq 2, L is ligand concentration (cysteine or serine), K_{ESB} is the dissociation constant for the external Schiff base, and ΔA_{457}^{obs} and ΔA_{457}^{max} are observed and maximum absorbance changes at 457 nm as a result of formation of the ESB.

Data for K_{ESB} vs pH were fitted to eq 3, while data for the pH dependence of the first-order rate of disappearance of the AA intermediate were fitted to eq 4.

$$\log y = \log\left(\frac{C}{1 + H/K_a}\right) \tag{3}$$

$$\log y = \log\left[\frac{Y_L + Y_H(H/K_a)}{1 + H/K_a}\right] \tag{4}$$

In eq 3, y is the observed value of $1/K_{ESB}$ obtained as a function of pH, C is the pH independent value of y. H is the hydrogen ion concentration, and K_a is the acid dissociation constant for an enzyme or amino acid functional group. In eq 4, y is k_{obs} measured at any pH, Y_L and Y_H are pH-independent values of the first-order rate constant for disappearance of the AA intermediate, and all other terms are as defined above.

Global fitting of the RSSF spectral data was carried out using the fitting program provided by OLIS and fitted to eq 5 to obtain first-order rate constants (k_{obs}) for the conversion of the ISB to AA.

$$A_t = A_0 e^{-k_{obs}t} + B_0 \quad (5)$$

In eq 5, A_t is the absorbance at time t, A_0 is the absorbance at time zero, and B_0 corrects for background absorbance. The rate constant, k_{obs}, was then plotted against pH and fitted to eq 3 to estimate the pK_a of the enzyme group involved.

Steady-State Fluorescence Measurements. Fluorescence measurements were carried out using a Fluoro-Max-3 fluorometer (HORIBA), equipped with a thermostated cell holder. Fluorescence spectra were corrected for the buffer contribution. Emission spectra, upon excitation at 298 nm, were collected from 310 to 550 nm, while emission spectra, upon excitation at 330 nm, were collected from 345 to 600 nm. Emission spectra, upon excitation at 412 nm, were collected from 425 to 650 nm. Excitation spectra, upon emission at 500 nm, were collected from 260 to 490 nm and were corrected for the spectrum of the xenon lamp. The excitation and emission slit widths were chosen on the basis of the protein concentration in order to keep the signal within the linear range of the instrument. The protein or ligand concentration in fluorescence experiments was selected to avoid any inner filter effect. Experiments were carried out in 100 mM K^+-Hepes buffer, pH 7, or 100 mM K^+-Ches buffer, pH 9.0, at 20 ± 0.5 °C.

RESULTS

Quality of the Structure. The final model comprises four dimers of OASS-B, with each dimer containing 586 residues (293 residues/monomer). Residues 294−303 are disordered and were not included in the model. The eight monomers in the asymmetric unit contain eight molecules of the cofactor PLP and 628 water molecules, which were introduced while monitoring the decrease in R_{free} using data to 2.3 Å resolution (Table 1). The free *R*-factor was calculated with 4.8% (8993 reflections) of the native data set aside prior to refinement and has a final value of 23.7%; the final value of the *R*-factor is 21.3%. The rmsd from ideal bond lengths and bond angles are 0.012 Å and 1.6°, respectively. A superposition of all eight monomers using the McLachlan fitting algorithm (*26*) yielded a rmsd of 0.34 Å comparing all atoms. The rmsd of the main chain atoms alone is 0.18 Å, while the rmsd of the side chain atoms alone is 0.46 Å. In a per residue comparison, including all atoms of the residue, the largest deviation is reported for Arg-184 with a rmsd of 2.25 Å. Thus, the backbone conformation and most side chain conformations between the eight monomers in the crystal structure are nearly identical.

The model was of good quality with 89.8% of the residues falling into the most favorable and 9.8% of the residues falling in the additionally allowed region of the Ramachandran plot. The stereochemistry was assessed using PROCHECK (*27*), and it was confirmed that no residues are in the disallowed regions.

Overall and Subunit Structure. OASS-B belongs to the β-family of vitamin B_6-dependent enzymes, which includes, among others, OASS-A, tryptophan synthase β-subunit, threonine synthase, and threonine deaminase. The overall structure of the dimer of holo-OASS-B is shown in Figure 1. The atoms of the two subunits in the dimer are related by a noncrystallographic 2-fold axis.

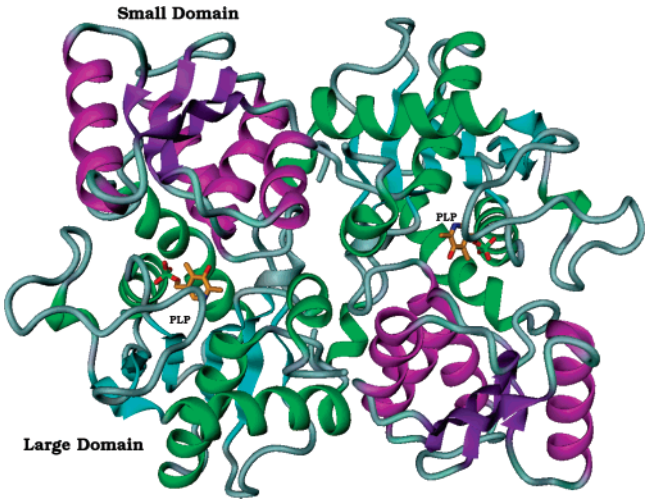

FIGURE 1: Schematic representation of the overall structure of the OASS-B dimer from *S. typhimurium*. α-Helices, 3_{10}-helices, and β-sheets in the small domain are colored in purple and violet, respectively, while those in the large domain are colored in green and cyan. PLP, represented in ball and stick model (orange), is buried inside the substrate-binding groove, which is the active site of the enzyme. The figure was prepared using the program DINO (http://www.dino3d.org).

The enzyme consists of a large domain and a small domain. The large domain has an interior β-sheet comprised of five parallel (β2, β7, β8, β9, and β10) β-strands and one antiparallel (β1) β-strand, surrounded by two α-helices on one side (α8 and α9) and three α-helices on the other side (α5, α6, and α7). The small domain also contains a β-sheet structure consisting of four β-strands (β3, β4, β5, and β6) surrounded by four α-helices (α1, α2, α3, and α4). Two β-turns, one from each monomer, overlap to form part of the subunit−subunit interface. Many of the active site residues that react with the cofactor, PLP, are situated at or near one end of the six-stranded β-sheet, forming the base of the active site cavity.

OASS-B, similar to OASS-A, contains a sub-domain, corresponding to residues 86−130, which moves to close the site along with movement of the substrate-binding loop (68-TSGN-71). A comparison of the location of the substrate-binding loop in the OASS-A and -B structures indicates that the unliganded structure reported herein is in an "open conformation" (*4*; see below).

The average temperature factor of the main chain atoms (N, C, C_α, and O) of all eight monomers is 46.3 Å^2 (Table 2). The values for individual monomers vary from 43.9 to 50.7 Å^2. There are a few regions with elevated temperature factors (>50 Å^2) of the C_α atoms, namely, the stretches around residues 15−30, 90−105, 110−140, 185−195, 195−205, and 205−220 (Figure 2). In addition, the last few residues of the model have elevated temperature factors, and the end of the sequence is disordered. The average temperature factors of the crystal structure of OASS-B are higher than those of the analogous structure of OASS-A in its open form (*4*; Figure 2). This is not simply an artifact of different crystal lattice contacts that would influence the average *B*-factors on surface loops that are involved in such contacts. Especially, the residues in the center of the structure show

Table 2: Average Temperature Factors and Crystallization Parameters for OASS-B and OASS-A Structures

protein	PDB code	space group	V_M (Å^3/Da)	solvent content (%)	average *B*-factor (Å^2)
S. typhimurium OASS-B	2JC3	*P*1	4.17	71.0	47.0
E. coli OASS-B [triple surface mutant (*7*)]	2BHT	$I4_1$	4.14	70.3	43.7
E. coli OASS-B [wild type (*7*)]	2BHS	$P6_522$	4.97	75.3	64.1
S. typhimurium OASS-A [wild type (*4*)]	1OAS	$P2_12_12_1$	2.83	56.5	35.3
S. typhimurium OASS-A [chloride-bound (*6*)]	1FCJ	$P2_12_12_1$	2.51	51.0	27.9
S. typhimurium OASS-A [closed conformation (*5*)]	1D6S	$P2_12_12_1$	2.82	56.5	33.6

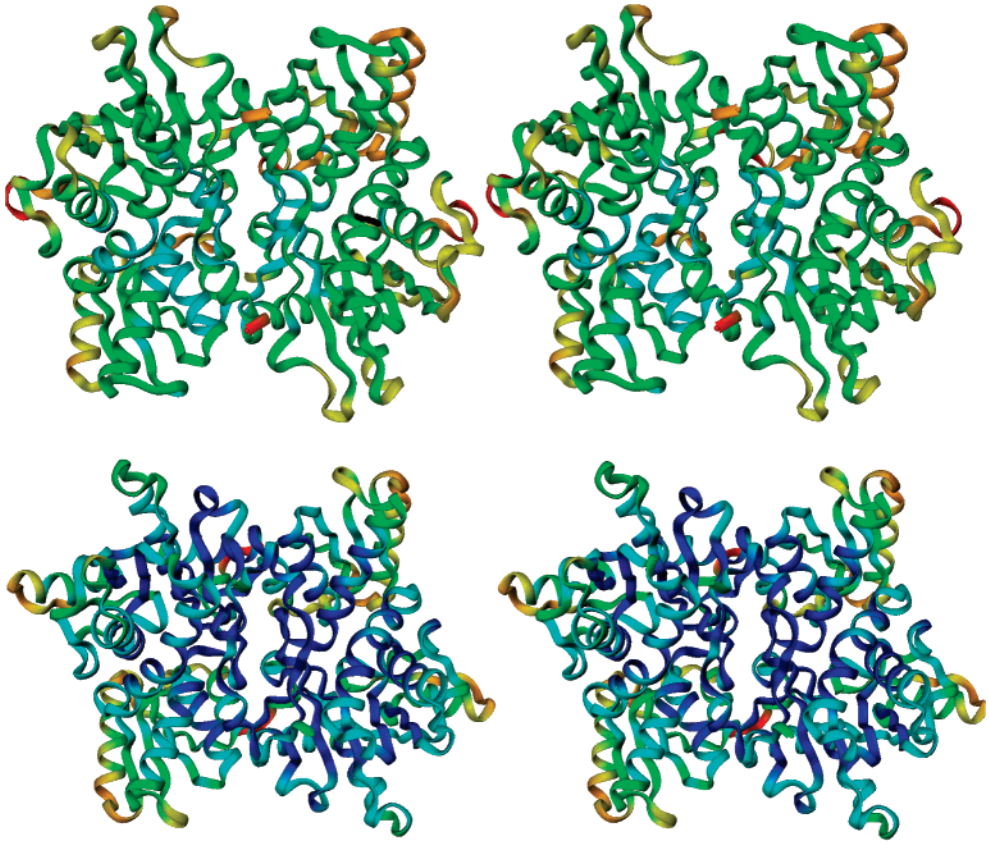

FIGURE 2: Comparison of the *B*-factors of OASS-B and OASS-A. The stereo representations of the C_α trace of the structures of OASS-B (top) and OASS-A in its open conformation [bottom; PDB ID 1OAS (*4*)] are color coded according to their *B*-factors. The color coding corresponds to *B*-factor values (in Å^2) of 9−23 (blue), 23−36 (cyan), 36−49 (green), 49−62 (yellow), 62−75 (orange), and 75−88 (red), respectively. The figure was prepared using the program DINO (http://www.dino3d.org).

increased temperature factors in the B-enzyme compared to the A-isoform (Figure 2), and these are the residues that are not involved in crystal lattice contacts. The crystal structures of OASS-B from *E. coli* (*7*) also have higher average *B*-factors compared to all other available crystal structures of OASS-A (*5*, *6*; Table 2) with the highest *B*-factors in the center of the molecules.

Coenzyme Binding Site. The coenzyme PLP is deeply buried inside the cleft between large and small domain (Figures 1 and 3), and the active site is accessible only via a narrow channel. The cofactor is linked to the ϵ-amino group of K41 via an imine linkage to form the ISB. The N1 nitrogen of the pyridine ring of PLP is within hydrogen-bonding distance to Oγ of S255 as observed in OASS-A (S272). The phosphate group of PLP interacts with the positive end of the dipole of α-helix 7 and the phosphate-binding loop (174-GTTGT-178). These residues form an extended hydrogen-bonding network, anchoring the phosphate moiety of PLP to the protein matrix. In this loop T176 is unique to OASS-B, which is replaced by G in OASS-A. The ^{31}P NMR chemical shift for unliganded OASS-A of 5.2 ppm, and a line width of 20 Hz, indicated a tightly bound dianionic phosphate group with its motion restricted to that of the protein (*25*). By analogy to OASS-A, the 5′-phosphate group in OASS-B is expected to be dianionic. H150, which is within hydrogen-bonding distance to a water molecule that donates a hydrogen bond to the 5′-phosphate, may be positively charged to provide near neutrality of the 5′-phosphate, identical to the arrangement in OASS-A. Finally, O3′ of the cofactor accepts a hydrogen bond from the side chain amide nitrogen of N71, part of the substrate-binding loop (Figure 3A).

The *si* face of the pyridine ring of PLP rests on a hydrophobic surface partially formed by V40 (Figure 3A), as also found in OASS-A. This residue prevents a tilt of the coenzyme pyridine ring toward the back of the active site and is partly responsible for the position of the cofactor. As in the A-isozyme, the *re* face of the ISB in OASS-B faces the active site entrance.

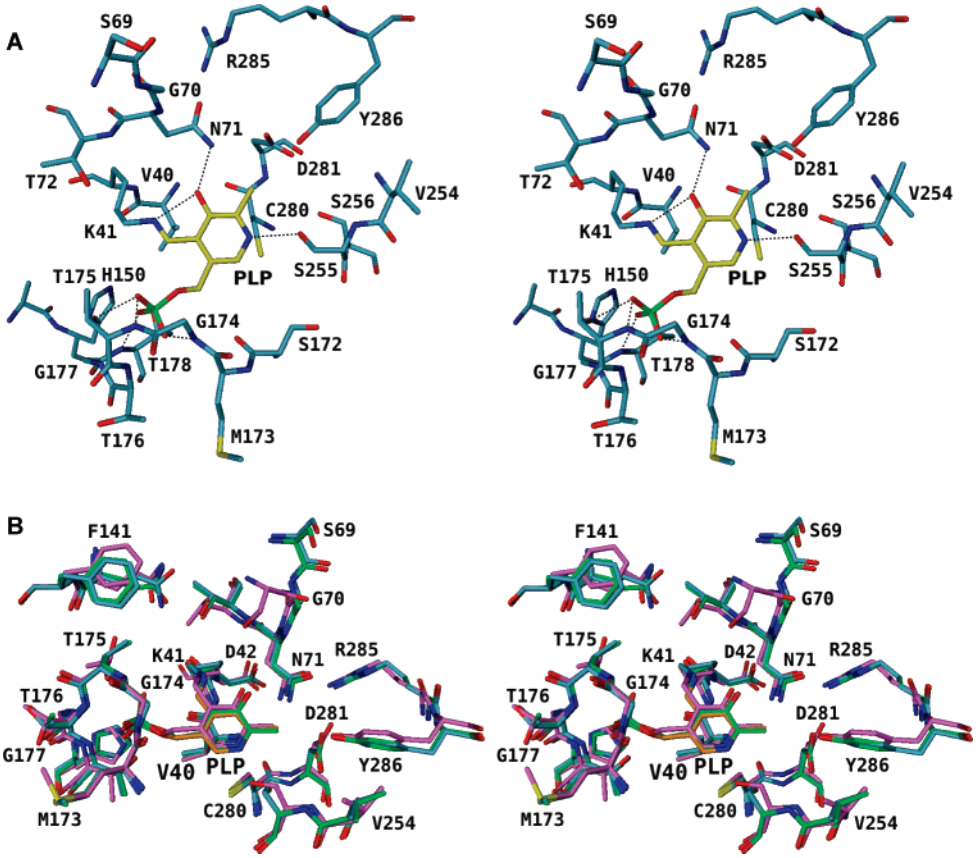

FIGURE 3: Stereo representation of the active site of OASS-B. (A) Active site conformation with the residues surrounding the PLP molecule. S255 is within hydrogen-bonding distance to N1 of the pyridine ring, and O3 of the pyridinium ring of PLP is within hydrogen-bonding distance to N71. Anchoring of the 5′-phosphate of PLP via an extended hydrogen bond network is also shown, where the three oxygen atoms of the 5′-phosphate are hydrogen bonded to residues T176, G177, and T178 of helix 7. Hydrogen bonds are shown as black stippled lines. (B) Active site region of OASS-B from *S. typhimurium* (gray) superpositioned on the active site of the wild-type *E. coli* OASS-B (green) and the Cys-rke surface mutant (violet) (*7*). *S. typhimurium* OASS-B resembles the wild-type *E. coli* OASS-B structure; the substrate-binding loop residues (Tyr-68−Asn-71) are in an "open" conformation. The surface mutant structure shows a "closed" conformation. The figure was prepared using the program DINO (http://www.dino3d.org).

Active Site Residues. A comparison of the active sites of the A- and B-isozymes indicates a less hydrophobic site overall in OASS-B due to the presence of two ionizable residues, D281 and C280 (*4*, *7*). D281 replaces S300 in OASS-A, is above the *re* face of the cofactor, and is within hydrogen-bonding distance to Y286 (Figure 3A). In addition, C280 replaces P299 in OASS-A and contributes to a more acidic character of the active site. Two arginine residues, R99 and R285, are found at or near the active site of both isozymes.

Finally, C42 in OASS-A is replaced by D42 in the B-isozyme. This residue is not part of the active site cavity itself but is adjacent to K41, the Schiff base lysine in the active site. In the A- and B-isozymes, C42 and D42, respectively, are directed away from the active site and into the protein structure. In the case of the A-isozyme, C42 participates in the pathway for transduction of the allosteric signal resulting from binding of small inorganic ions to a site at the dimer interface (*6*, *28*). An allosteric binding site at the dimer interface is not apparent in OASS-B, although functional data (*2*) indicate an inhibitory effect of chloride ions on OASS-B activity. D42 is deeply buried in the protein matrix, and in the event the carboxyl side chain is ionized, there is no possibility of charge compensation by ionic interaction. Ionization of D42 will therefore generate an isolated negative charge in the interior of the protein, and its pK_a is expected to be quite high. The only way to compensate for a negative charge resulting from deprotonation of D42 would be from dipolar interactions, and this would require a major rearrangement of the protein structure that cannot be predicted. Whether this residue in its ionized form would induce a conformational change similar to the one observed for C42 in the inhibited form of the A-isozyme remains highly speculative (*6*).

Absorbance Spectra of OASS-A and OASS-B. The internal aldimine absorbance spectra of OASS-A and -B, measured at pH 7.0, exhibit a band centered at 412 and 414 nm, respectively (Figure 4A). This peak indicates that the predominant tautomer of the internal aldimine is the ketoenamine, and the imine nitrogen of the cofactor is protonated allowing the formation of an intramolecular hydrogen bond with the 3′-oxygen atom of PLP and the conjugation of the π system of the imine with the pyridine ring (*16*, *25*, *29*). The ratio between the intensity at 280 and 412 nm or 414 nm is 3.4−3.6 for the A-isozyme (*25*) and 4.0−4.2 for the B-isozyme. This difference reflects the presence of two tryptophan residues, W50 and W161, in the A-isozyme, and three tryptophans, W28, W159, and W212, in the B isoform. The absorption band at 412−414 nm is asymmetric and broader on the blue side (Figure 4A), suggesting the presence of species absorbing at lower wavelengths. In the spectral region between 320 and 350 nm several PLP derivatives

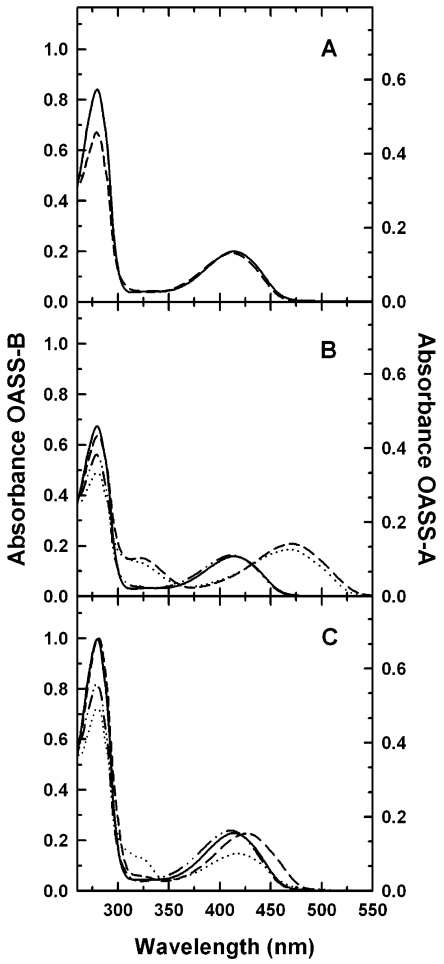

FIGURE 4: Absorbance spectra of OASS-A and OASS-B in the absence and presence of ligands. (A) Absorbance spectra of solutions containing either 17.4 μM OASS-A (dotted line) or 17.4 μM OASS-B (solid line) and 100 mM Hepes, pH 7. (B) Absorbance spectra of solutions containing either 13.8 μM OASS-A, in the absence (dash-dot-dot line) or presence of 10 mM OAS (dotted line), or 13.8 μM OASS-B, in the absence (solid line) or presence of 10 mM OAS (dashed line), and 100 mM Hepes, pH 7. (C) Absorbance spectra of solutions containing either 19.9 μM OASS-A, in the absence (dash-dot-dot line) or presence of 161 mM L-serine (dotted line), or 19.9 μM OASS-B, in the absence (solid line) or presence of 161 mM L-serine (dashed line), and 100 mM Ches, pH 9. Experiments were carried out at 20 $\pm$ 0.5 °C.

absorb, including the enolimine tautomer of the ISB and ESB, the *gem*-diamines, and species formed due to covalent modifications of the coenzyme. In the structurally related enzyme tryptophan synthase, a broad band at 335 nm was attributed to the enolimine tautomer of the internal aldimine (*30*), a species stabilized with respect to the ketoenamine by a less polar environment (*13*). A similar assignment can be proposed for the weak band at 330 nm of OASS-B (Figure 4A). Furthermore, the band at 414 nm of the internal aldimine of OASS-B increases as a function of pH with a concomitant decrease in the band at 330 nm (data not shown), indicating that the deprotonation of some residues in the active site stabilizes the ketoenamine species. Interestingly, the spectrum of the OASS-A ISB is pH independent; thus the ionizable residue is either missing or has a different location.

The reaction of OASS with the substrate *O*-acetylserine (OAS) causes the disappearance of the band at 412−414 nm and the concomitant formation of bands at 325 and 470 nm for OASS-A (*3*, *29*) and 327 and 472 nm for OASS-B (Figure 4B). These bands are attributed to the enolimine and ketoenamine tautomers of the α-aminoacrylate Schiff base, formed upon the β-elimination of acetate (Scheme 1) (*3*, *25*).

Upon binding of the substrate analogue L-serine to OASS-A, the band at 412 nm shifts to 418 nm with an intensity decrease, while a new band, centered at 325 nm, appears (Figure 4C). In the case of the B-isozyme, the reaction with L-serine results in a shift of the 414 nm band to 427 nm with no intensity change and a very weak intensity increase at 325 nm (Figure 4C). The observed absorbance increases at ~470 nm for both OASS-A and OASS-B are fully accounted for by the red shift of the band and are not due to formation of the AA. Consistent with this interpretation, assays of OASS-B in the presence of L-serine, NADH, and lactate dehydrogenase did not reveal any production of pyruvate (data not shown), which is formed via hydrolysis of the resulting AA.

pH Dependence of K_{ESB} Obtained from Ultraviolet−Visible Spectral Titrations. UV−visible absorbance spectra for the reaction of increasing concentrations of L-serine with OASS-B at pH 9.3 are shown in Figure 5A. The λ_{max} for the absorbance change, obtained from difference spectra in the presence and absence of serine, is at 457 nm, and ΔA_{457} was used to calculate the K_{ESB}. Experiments were repeated as a function of pH, and a plot of pK_{ESB} vs pH (Figure 5B) has a limiting slope of +1 and yields a pK_a value of 7.7 $\pm$ 0.6. The pH-independent value, above pH 8.0, of K_{ESB} for serine is about 30 $\pm$ 6 mM.

The UV−visible absorbance spectra of OASS-B in the presence of different concentrations of L-cysteine at pH 9.4 are shown in Figure 5C. Addition of L-cysteine results in a significant decrease in absorbance at 414 nm and a shift to 422 nm, concomitant with an increase in absorbance at 325 nm. The K_{ESB} with L-cysteine was calculated using the increase in A_{457}, and a plot of pK_{ESB} versus pH was obtained (Figure 5D). A pK_a value of 6.9 $\pm$ 0.3 was estimated from the pK_{ESB} profile, and a pH-independent value of K_{ESB} of 3.0 $\pm$ 0.3 mM was estimated above pH 7.5.

OAS:Acetate Lyase Activity. The AA, preformed by reacting the enzyme with equimolar amounts of OAS, is unstable. Time-dependent absorbance spectra were collected to monitor the disappearance of the α-aminoacrylate intermediate at 472 nm and the appearance of the free enzyme at 414 nm as a function of pH. The 472 nm band disappears with time in a first-order process, indicating the displacement of AA, i.e., the presence of OAS:acetate lyase activity in which the products of the reaction are free enzyme, pyruvate, and ammonia, as was observed with the OASS-A isozyme (*25*). The value of k_{obs} decreases from a high pH constant value of 4.4 $\pm$ 1.7 s^{-1} to a low pH constant value of 0.090 $\pm$ 0.008 s^{-1}. A pK of 9.1 $\pm$ 0.6 is estimated from a fit of the data (Figure 6).

Initial Velocity Studies. Steady-state kinetic parameters for OASS-B are summarized in Table 3. OAS was used as the amino acid substrate, and TNB was used as the nucleophilic substrate in place of bisulfide, the natural substrate. Comparison of the observed kinetic parameters with those obtained previously (*2*) indicates a close agreement.

Rapid-Scanning Stopped-Flow Studies. RSSF measurements were carried out to obtain information on the identity and rates of appearance and decomposition of transient species in the pre steady state. Kinetic parameters for the

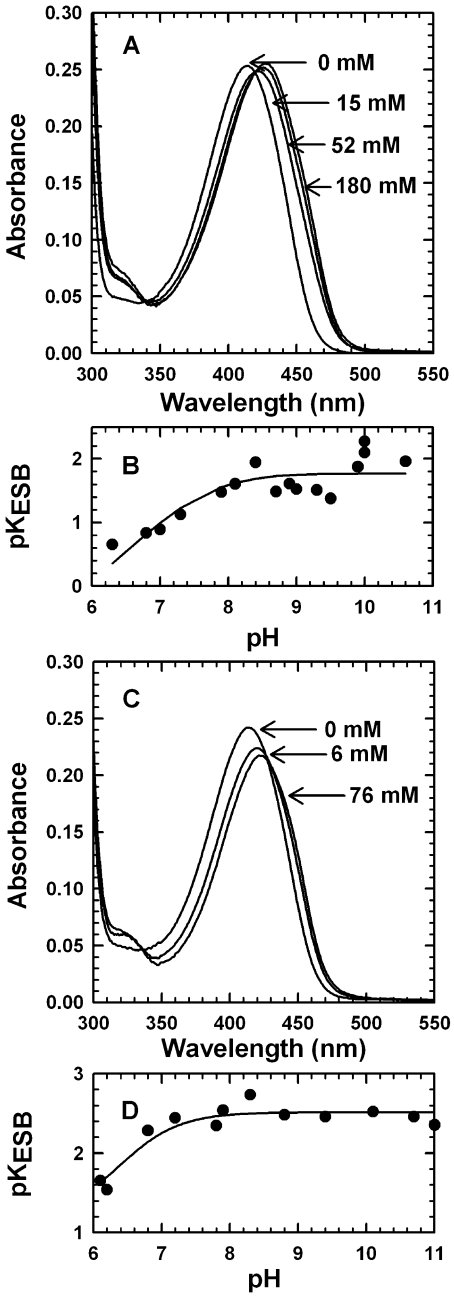

FIGURE 5: External Schiff base formation with serine and cysteine. (A) Titration of OASS-B with L-serine. Absorbance spectra were measured with 21 μM OASS-B at pH 9.3 and 25 °C. Serine concentrations are as indicated in the figure. (B) Dependence of pK_{ESB} on pH. The curve has a limiting slope of +1 on the acid side with a pK_a value of 7.7 ± 0.6. (C) Titration of the enzyme with L-cysteine. Absorbance spectra were measured with 21 μM OASS-B at pH 9.4 and 25 °C. Cysteine concentrations are as indicated in the figure. (D) Dependence of pK_{ESB} on pH. The curve has a limiting slope of +1 on the acid side with a pK_a value of 6.9 ± 0.3. For (B) and (D), points are experimental values, while the curve is theoretical, based on the fit to eq 3.

formation of the AA for the first half of the OASS-B reaction were obtained as a function of pH under conditions where ISB reacts with OAS. In Figure 7A, spectra 1 and 9 are for ISB and AA, respectively. The spectra exhibit clear isosbestic points, which suggest that the internal Schiff base (λ_{max} at 414 nm) is converted to the two tautomeric forms of AA with λ_{max} values of 327 and 472 nm. The rate constants obtained from the time courses at 414 and 472 nm are identical (Figure 7B), suggesting that no additional detectable

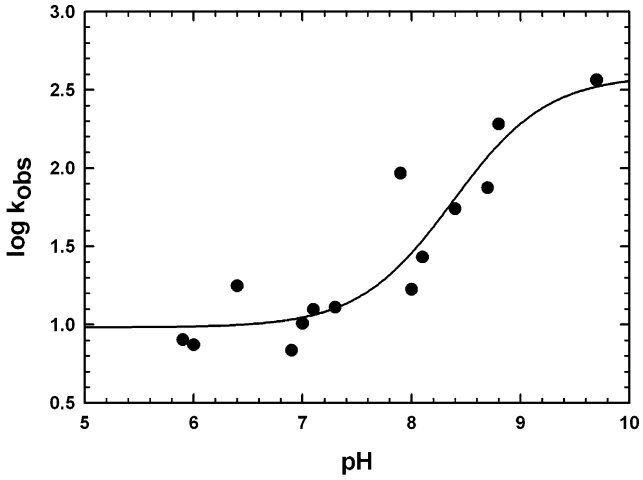

FIGURE 6: pH dependence of the decay of the α-aminoacrylate intermediate. Points are experimental values, while the curve is from a fit of the data to eq 3. Values of k_{obs} at high and low pH are 4.4 ± 1.7 and 0.090 ± 0.008 s^{-1}, respectively, and a pK of 9.1 ± 0.6 is estimated.

Table 3: Steady-State Kinetic Parameters for OASS-B at pH 7.0

V/E_t (s^{-1})	7.0 ± 1.5
$V/K_{OAS}E_t$ ($M^{-1}\,s^{-1}$)	(3.5 ± 1.3) × 10^4
$V/K_{TNB}E_t$ ($M^{-1}\,s^{-1}$)	(3.7 ± 1.3) × 10^4
K_{OAS} (mM)	0.20 ± 0.06
K_{TNB} (mM)	0.19 ± 0.05

intermediate builds up at a significant concentration between ISB and AA under the conditions used. The first-order rate constant (k_{obs}) was a linear function of the OAS concentration over the range 0.05−10 mM. Therefore, a linear function was used to fit the dependence of k_{obs} on OAS concentration to obtain the second-order rate constant (k_{max}/K_{ESB}), and this was repeated at different pH values. A plot of log k_{max}/K_{ESB} versus pH (Figure 7C) has a limiting slope of +1. An estimate of the pK_a is ≥6.5. The RSSF spectra of the L-serine or L-cysteine external Schiff bases show a shift in λ_{max} from 414 nm (for the ISB from Figure 4) to 427 and 422 nm, respectively, in the dead time of the instrument (data not shown). No formation of the AA was observed at 472 nm at all concentrations tested at any pH value from 6.0 to 10.0.

Steady-State Fluorescence Spectra of OASS-A and OASS-B. The tryptophans, W50/W28 and W161/W159, are conserved in OASS-A and OASS-B and are located in similar positions. The third tryptophan, W212, which has no homologue in the A-isozyme, is near the active site, 15 Å from PLP, and is buried in the protein matrix. Upon excitation of tryptophan at 298 nm, the fluorescence emission spectrum of OASS-B shows striking differences with respect to OASS-A (Figure 8A). The OASS-B emission spectrum exhibits major bands centered at 336 and 425 nm, while the OASS-A spectrum shows peaks centered at 338 nm and about 500 nm, in agreement with previous studies (*9*, *10*). The emission spectrum of OASS-B, obtained by the direct excitation at 330 nm (Figure 8B), exhibits a single band at 425 nm, whereas that of OASS-A exhibits emission bands both at about 400 and at 500 nm. Upon excitation of the ketoenamine tautomer of the internal aldimine at 412 nm, the OASS-B emission spectrum shows a band centered at 511 nm, 6 nm red shifted with respect to that of OASS-A (Figure 8C). Under the same experimental conditions, the

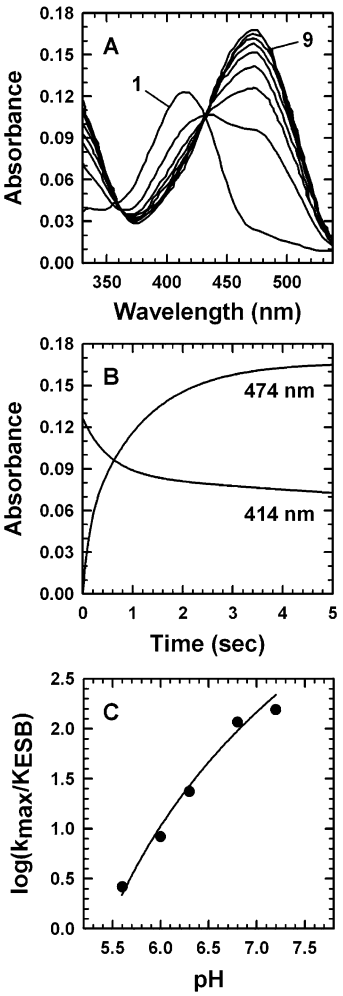

FIGURE 7: Rapid-scanning stopped-flow spectra obtained upon reaction of OASS-B and OAS. (A) Spectrum 1 represents the free enzyme, and spectrum 9 represents the AA. The time difference between each spectrum is 0.6 s. The concentration of OASS-B was 10 μM and OAS was 0.1 mM. The reaction was carried out in 200 mM Mes, pH 6. (B) Time courses for the disappearance of the free enzyme measured at 414 nm and appearance of the AA measured at 472 nm. Rate constants were identical. (C) pH dependence of $\log(k_{max}/K_{ESB})$. The curve has a limiting slope of +1 on the acid side and a fit of the data to eq 3 gives an estimate of the p$K_a \geq 6.5$. The points are experimental values, while the curve is theoretical, based on the fit to eq 3.

intensity of the peak at 505 nm for the A-isoform is 2-fold higher than the intensity at 511 nm for the B-isozyme, indicating a higher quantum yield and/or fractional population for the ketoenamine tautomer of OASS-A. The enolimine emission of OASS-A, instead, is lower than that of OASS-B (Figure 8B). The excitation spectra collected for OASS-A and OASS-B provide a consistent pattern (Figure 8D).

As previously observed (*11*, *24*), upon excitation at 298 nm, in the presence of L-serine, the cofactor emission band of OASS-A exhibits a blue shift to 490 nm and an intensity increase with respect to the internal aldimine emission spectrum (Figure 9A), while the Trp emission band is red shifted to 340 nm, maintaining almost the same intensity. Upon excitation at 298 nm, the emission spectrum of OASS-B, in the presence of L-serine, exhibits a band centered at 507 nm, not present in the ISB spectrum, without any significant effect on the emission maxima at 336 and 425 nm (Figure 9A). By exploiting the dependence of the emission intensity at 507 nm on L-serine concentration (data not shown), the dissociation constant of the L-serine−OASS-B complex was measured and found to be in close agreement with that determined from absorption data (Figure 5B) and that measured for OASS-A (*24*). The difference in emission properties between internal and external aldimine of OASS-B is even more evident upon direct excitation of the enolimine tautomer at 330 nm, with the appearance of a broad shoulder at about 500 nm without any change in the intensity and position of the band at 425 nm (data not shown). The enhancement in the emission band of the ketoenamine tautomer is confirmed by the direct excitation of the ketoenamine tautomer at 412 nm (Figure 9B). The emission of the external aldimine shows an increase of more than 6-fold and 2-fold with respect to the emission of the internal aldimine for OASS-B and OASS-A, respectively. For both isoforms, the emission maxima are blue shifted with respect to the ISB forms, especially for OASS-A. The excitation spectra for OASS-A and B, recorded for emission at 500 nm, exhibit major peaks at 280 and about 420−430 nm, confirming that the ketoenamine excitation band is red shifted for OASS-B with respect to OASS-A (Figure 9C).

The binding of acetate to the α-carboxylate subsite of the OASS-A active site, behaving as a dead-end inhibitor, exhibits a weak effect on the OASS-A absorbance spectrum, with a slight red shift of the ketoenamine tautomer peak (*10*, *11*). Upon addition of acetate, the OASS-B absorption spectrum shows the same red shift of the ketoenamine tautomer peak (data not shown). In the presence of acetate, upon excitation at 298 nm, the emission band of OASS-B at 335 nm is not significantly affected, while a band at 495 nm appears with the concomitant blue shift and decrease in the intensity of the emission band at 425 nm (Figure 10A). The emission spectra recorded in the presence of different concentrations of acetate show an isoemissive point at 458 nm, suggesting that ligand binding causes a change in the relative concentration of the enolimine and ketoenamine tautomers of the internal aldimine. Specifically, acetate seems to favor the ketoenamine tautomer. This conclusion is also supported by the direct excitation of the enolimine tautomer at 330 nm, in the presence of acetate (Figure 10B). The emission spectrum shows that the peak attributed to the enolimine tautomer blue shifts from 428 to 425 nm and decreases in intensity with the concomitant appearance of a broad shoulder centered at about 510 nm. Upon excitation at 412 nm, the emission spectrum shows an increase in the band at 510 nm (Figure 10C). In agreement with the emission spectrum, the excitation spectrum, recorded for emission at 500 nm, exhibits peaks at 415 and 279 nm (Figure 10D).

DISCUSSION

Conformation of OASS-B. Three conformations of OASS-A are known, an open form (ISB; *4*), a closed form (ESB of the K41A mutant enzyme with methionine; *5*), and an inhibited form with Cl^- bound to an allosteric site at the subunit interface (*6*). The conformational change to close the site is triggered by binding of the substrate α-carboxylate to the substrate-binding loop (residues 68−71), specifically to the side chain of S69 in OASS-A, which moves by more than 7 Å as the active site closes. Fluorescence data suggest that a similar event is caused by acetate which abortively

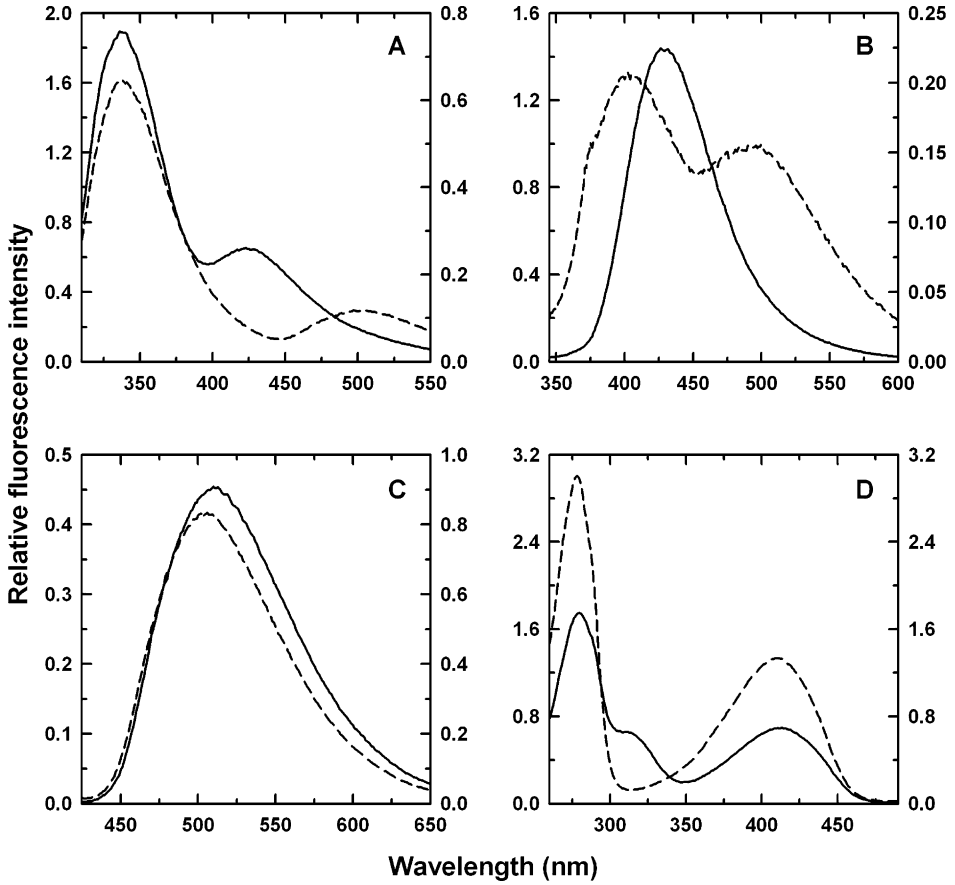

FIGURE 8: Steady-state fluorescence spectra of OASS-A and OASS-B. Spectra were recorded in 100 mM Hepes, pH 7, at 20 ± 0.5 °C. The concentration of OASS-A and OASS-B was 2 μM. The *y*-axis scale on the left refers to the emission intensity of OASS-B; that on the right, to OASS-A. (A) Fluorescence emission spectra upon excitation at 298 nm of OASS-A (dashed line) and OASS-B (solid line) ($slit_{ex}$ = 4 nm, $slit_{em}$ = 4 nm). (B) Fluorescence emission spectra upon excitation at 330 nm of OASS-A (dashed line) and OASS-B (solid line) ($slit_{ex}$ = 5 nm, $slit_{em}$ = 5 nm). (C) Fluorescence emission spectra upon excitation at 412 nm of OASS-A (dashed line) and OASS-B (solid line) ($slit_{ex}$ = 5 nm, $slit_{em}$ = 5 nm). (D) Fluorescence excitation spectra for emission at 500 nm of OASS-A (dashed line) and OASS-B (solid line) ($slit_{ex}$ = 5 nm, $slit_{em}$ = 5 nm).

occupies the α-carboxylate subsite (*11*). The result is the induction of a large global conformational change with rotation of the "movable domain" comprising residues 86−130 (Figure 11). The structure of OASS-B presented in this report exhibits the substrate-binding loop in a position suggesting the open form, expected for the unliganded enzyme form, and conforms very closely to the structure of the wild-type enzyme from *E. coli* (97% identity to the *S. typhimurium* enzyme) (*7*). Of interest, the structure of the *E. coli* OASS-B with a surface mutation (CysM-rke) exhibits, for some unknown reason, a closed conformation on the basis of the position of the substrate-binding loop (Figures 3B and 11) (*7*). As for OASS-A, S69 is expected to be one of the main residues responsible for ligand or inhibitor binding. The >7 Å movement of S69 in the substrate-binding loop observed for OASS-A upon substrate binding is anticipated, on the basis of the structures available, for S69 of OASS-B.[2]

Interpretation of pH Dependence of Spectral Changes and pK_{ESB} Profiles. Spectral changes observed with the B-isozyme are similar to those of the A-isozyme but differ in their pH and ligand concentration dependence. An overview of the tautomeric equilibria of the ISB and ESB is shown in Scheme 1. The ISB exists as a mixture of the ketoenamine and enolimine tautomeric forms, as do the ESB of OAS, serine, lanthionine [formed upon addition of cysteine to free enzyme (*24*)], and (AA). As discussed above, the tautomeric equilibria of OASS-B are pH dependent. The spectrum of the ISB at high pH favors the ketoenamine tautomer compared to low pH, while the opposite is true for the ESBs (unpublished results). Similar data obtained for the A-isozyme exhibit pH independence in both cases. These data suggest that a residue in the active site of the B-isozyme, that is not present in the A-isozyme, once deprotonated, affects the tautomeric distribution of the cofactor. The pK_a for the residue titrated is ≥7.0, and of the two ionizable residues that are unique to the active site of OASS-B, D281 and C280, it is likely that the thiol/thiolate titration of C280 is responsible for the change. Of interest, C280 is behind the cofactor (*si* face) and in the vicinity of the pyridinium nitrogen (3.4 Å). The pyridine nitrogen of PLP in OASS-B likely receives a hydrogen bond from S255 as proposed for S272 in OASS-A. As a result the pyridine nitrogen is neutral in both cases. As the pH is increased and C280 becomes ionized, the increased charge in the site would favor the ketoenamine tautomer.

However, the covalent imine linkage between PLP and K41 is absent in the ESBs, and the coenzyme is expected to

[2] S69 in OASS-A was initially erroneously assigned as N69 (*4*) and later corrected by referring to the original sequencing gels (N. M. Kredich, personal communication).

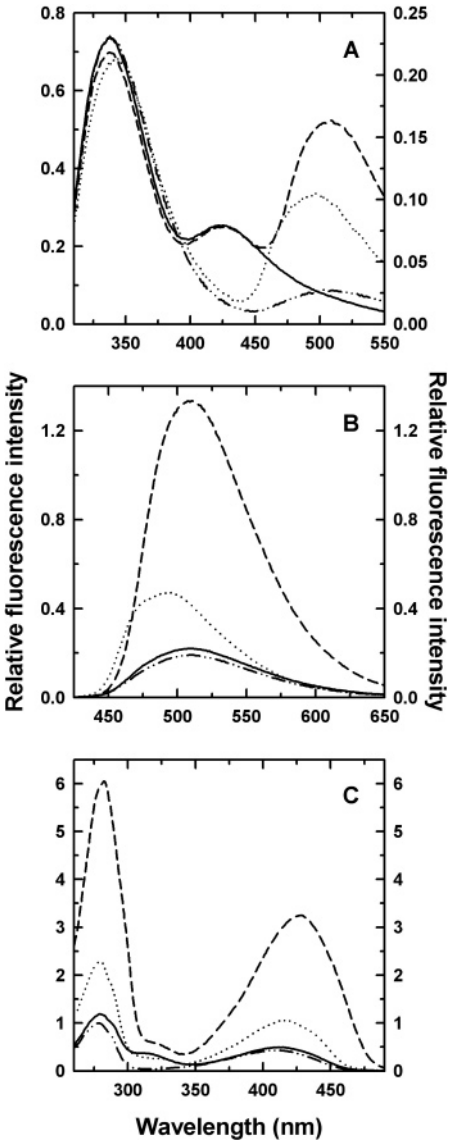

FIGURE 9: Steady-state fluorescence spectra of OASS external aldimine with L-serine. Spectra were recorded in 100 mM Ches, pH 9, at 20 ± 0.5 °C. The concentration of OASS-A and OASS-B was 2 μM. For OASS-B spectra were recorded in either the absence (solid line) or presence (dashed line) of 165 mM L-serine. For OASS-A spectra were recorded in either the absence (dash-dotted line) or presence (dotted line) of 165 mM L-serine. The *y*-axis scale on the left refers to the emission intensity of OASS-B; that on the right, to OASS-A. (A) Fluorescence emission spectra upon excitation at 298 nm ($slit_{ex}$ = 3 nm, $slit_{em}$ = 3 nm). (B) Fluorescence emission spectra upon excitation at 412 nm ($slit_{ex}$ = 3 nm, $slit_{em}$ = 3 nm). (C) Fluorescence excitation spectra for emission at 500 nm ($slit_{ex}$ = 3 nm, $slit_{em}$ = 3 nm).

tilt compared to its position in the ISB. The increased proximity to the pyridine nitrogen of the thiolate of C280 as the ESB is formed would be expected to affect the tautomeric equilibrium somewhat differently. The pyridine nitrogen might be expected to accept the proton from S255 to help neutralize the charged thiolate, which would favor the neutral imine of the enolimine consistent with this species being slightly more favored at high pH (see below) (the increase in negative charge of S255 might be neutralized by dipolar interactions of other side chains and/or water molecules). This aspect will have to await additional experimental evidence.

In the case of OASS-A, addition of serine to the ISB results in a decrease in the absorbance of the ketoenamine tautomer and a red shift of the remaining absorbance from 412 to 418 nm, concomitant with an increase in the absorbance of the enolimine tautomer that signals formation of the ESB (*24*; Figure 4C). Addition of cysteine to the ISB resulted only in a red shift to 418 nm. The pH dependence of K_{ESB} of both amino acids exhibited the presence of two groups that must be unprotonated for optimum formation of the ESB. In order to form the ESB, the α-amine of the amino acid must be neutral to act as a nucleophile to attack C4′ of the ISB. There was also the requirement for an enzyme group with a pK_a of about 7.0 to be unprotonated; this enzyme residue is thought to be involved in a pH-dependent conformational change. In the case of cysteine, the requirement for an additional group with a pK_a of about 8.0 that must be protonated was also observed; this was attributed to the side chain thiol of cysteine (*24*). The pH dependence of K_{ESB} for OASS-B is significantly different. Formation of the cysteine ESB at pH 9.4 is accompanied by a decrease in the absorbance of the ketoenamine tautomer of the ISB and a red shift in the absorbance maximum to 422 nm (Figure 5C), concomitant with an increase in the absorbance at 325 nm, suggesting a preference for the neutral species, similar to the changes observed for the AA at pH 10.0 (data not shown) and also very similar to the formation of the serine ESB of the A-isozyme. On the other hand, formation of the serine ESB is qualitatively identical to that observed for the cysteine ESB of the A-isozyme with the exception that a slight increase in the absorbance at 330 nm is also observed (Figure 5A), suggesting the neutral species is somewhat more favored at pH 9.3. Data suggest that the preference for the neutral enolimine is not as pronounced in the case of the serine ESB, probably a result of the ionization state of the thiol of cysteine as its ESB is formed.

The main difference between the A- and B-isozymes, however, is in the pH dependence of the K_d for the ESB. In the case of the A-isozyme, the affinity of the enzyme for serine increases when an enzyme group with a p*K* of about 7.0 and the α-amine of the amino acid are unprotonated (*24*). The same is true for the pH dependence of the cysteine K_d, with the additional requirement of a neutral thiol on the ligand. In the case of the B-isozyme, the only group titrated is the enzyme group with a p*K* of about 7.0. On the basis of the data, it would appear that the protonation states of the α-amine of the amino acid and the thiol of cysteine are not important for optimum ESB formation. However, since a neutral α-amine is required for nucleophilic attack on C4′ in ESB formation, the results seem contradictory and suggest a compensatory effect. That is, as the amine of the amino acid is deprotonated, favoring formation of the external Schiff base, a second group must be titrated, giving an enzyme form that is unfavorable for ESB formation. As discussed above, there is an enzyme group in the ISB which, when titrated, gives a shift in the tautomeric equilibrium as a result of increased negative charge in the active site (it is suggested that this group may be C280); deprotonation of C280 may disfavor ESB formation. The pK_a for the enzyme group should be similar to the amine pK_a. Test of this hypothesis will have to await further study.

α-*Aminoacrylate Formation and OAS:Acetate Lyase Activity*. The addition of OAS to the free enzyme results in the

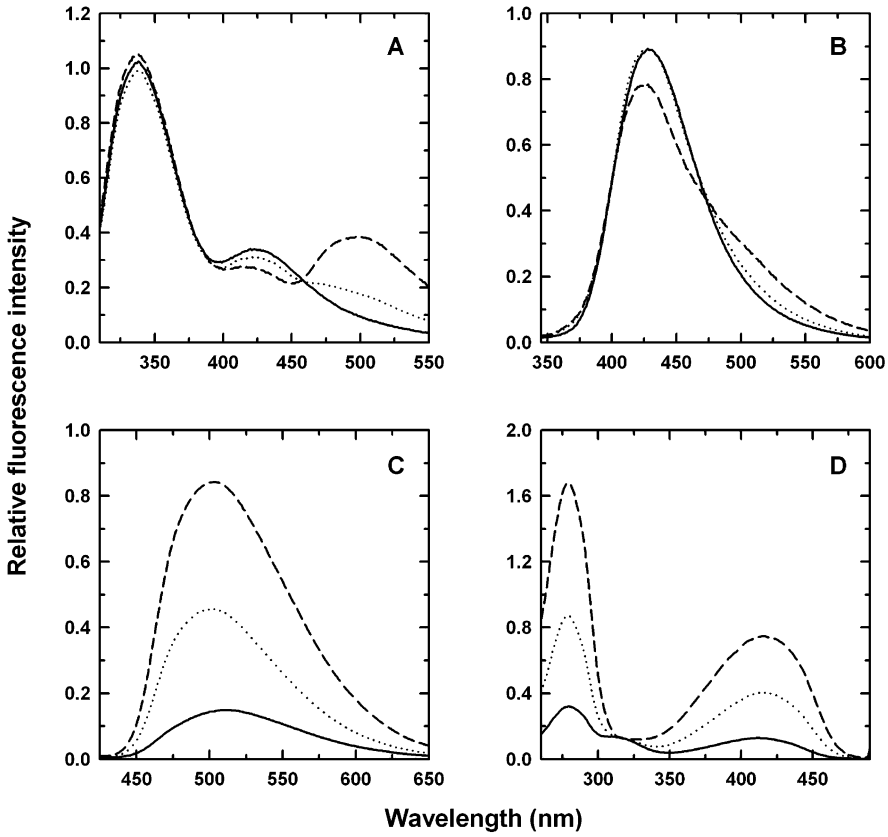

FIGURE 10: Steady-state fluorescence spectra of OASS-B in the presence of acetate. Spectra were recorded in 100 mM Hepes, pH 7 at 20 ± 0.5 °C. The concentration of OASS-B was 2.7 μM. Spectra were recorded in either the absence (solid line) or presence of 817 mM (dotted line) and 5 M acetate (dashed line). (A) Fluorescence emission spectra upon excitation at 298 nm ($slit_{ex}$ = 3 nm, $slit_{em}$ = 3 nm). (B) Fluorescence emission spectra upon excitation at 330 nm ($slit_{ex}$ = 4 nm, $slit_{em}$ = 4 nm). (C) Fluorescence emission spectra upon excitation at 412 nm ($slit_{ex}$ = 5 nm, $slit_{em}$ = 5 nm). (D) Fluorescence excitation spectra for emission at 500 nm ($slit_{ex}$ = 5 nm, $slit_{em}$ = 5 nm).

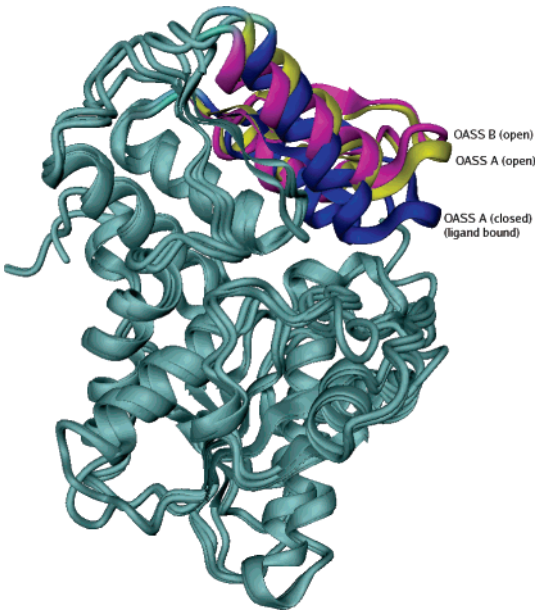

FIGURE 11: Superposition of the OASS-B monomer on the OASS-A native and closed forms. The domains in purple, yellow, and blue represent the structures of OASS-B, OASS-A open, and OASS-A closed, respectively. The recent structure of OASS-B resembles the OASS-A open conformation. The figure was prepared using the program DINO (http://www.dino3d.org).

formation of the AA and the production of acetate. In the absence of the nucleophilic substrate, the enzyme catalyzes a β-elimination reaction in which the AA decomposes to free enzyme, pyruvate, and ammonia. In the case of the A-isozyme, the elimination reaction occurs at a pH-independent rate of 0.1 s^{-1}. The reaction was interpreted to reflect transimination by K41 to displace α-aminoacrylate, which decomposes in solution to give pyruvate and ammonia (*25*). The pH dependence of the first-order rate constant gives a pK_a of 8.2 for OASS-A, which was also observed in the pH−rate profile for V/K_{TNB}, attributed to K41, which must protonate the product ESB that forms upon nucleophilic attack by the thiolate of TNB prior to product release (*25*). Consistent with the increased turnover number of the B-isozyme (≥10-fold) compared to that of the A-isozyme, the rate constant for decomposition of the AA intermediate is about 40-fold higher for OASS-B. In addition, the estimated pK_a of K41 is 9.1, about a pH unit higher than that of OASS-A, likely due to the increase in negative charge in the active site of OASS-B (see above).

Unlike data obtained for the A-isozyme, the first-order rate constant for decomposition of the AA in OASS-B decreases from a constant value at high pH above the pK_a of Lys-41 to another pH-independent value at low pH, approximately 50-fold lower than that at high pH. This behavior was also noted for the S272A mutant of OASS-A, which has a turnover number $^1/_{50}$th that of the wild-type enzyme (*31*). The authors attributed the low pH behavior as an attack by water on the AA to give the serine ESB. Serine is a very slow substrate for OASS-A (rate constant is in $days^{-1}$; *32*) with a very high dissociation constant for the serine ESB at

low pH (*24*). This explanation likely also applies in the case of the B-isozyme. Serine may be a somewhat better substrate for the B-isozyme. If it is ≥10-fold better for the B-isozyme than the A-isozyme, consistent with the difference in turnover numbers of the two isozymes, the rate constant would be in terms of h^{-1}.

As found for the A-isozyme, there is no evidence for formation of the AA with cysteine as the ligand, even though it is a product of the reaction of OAS with bisulfide. Data likely indicate a rapid transient appearance of the AA, which is attacked by the thiol of an additional cysteine to give the lanthionine external Schiff base as found for the A-isozyme (*33*) (confirmation will require additional experimentation). The rate constants for appearance and disappearance of the AA, if it forms, with cysteine as the substrate must be very fast, since no buildup of the intermediate is seen in rapid-scanning stopped-flow experiments (see above).

Reaction Rate in the Steady-State and Pre-Steady-State. As shown previously (*2*), and in this study, the B-isozyme exhibits a much faster rate of catalysis than the A-isozyme. The ratios of V/E_t, $V/K_{OAS}E_t$, and $V/K_{TNB}E_t$ with the OAS/TNB reactant pair are 12.5, ~1000, and 40, respectively, in favor of the B-isozyme. The reason for the faster rate in the case of OASS-B might be associated with higher protein flexibility, as suggested by the higher temperature factors of OASS-B relative to OASS-A (Figure 2 and Table 2).

Interpretation of the pre-steady-state studies, as discussed above, is relatively straightforward. Data reflect a rapid conversion of the ISB to the AA intermediate. The first-order rate constant measured in the pre-steady-state for the first half-reaction increases with increasing pH and exhibits a pK_a on the acid side of the pH−rate profile. Since the rate of formation of the AA is very fast, limited data were collected at pH values higher than 7.0. As a result, the pK_a of the group observed was not calculated but is ≥6.5, similar to that observed for the A-isozyme, and is attributed to an enzyme residue that is required unprotonated for optimum conformation of the active site (*34*, *35*).

In the case of the A-isozyme, with cysteine as a substrate, the AA was observed transiently in the pre-steady-state, since it reacts with another cysteine molecule to form the lanthionine ESB (*32*, *33*). In an attempt to detect intermediates along the reaction pathway, and to determine whether serine and cysteine served as substrates, RSSF studies were carried out with the B-isozyme and the two amino acids. As is true with the A-isozyme, no reaction was detected with the B-isozyme, nor were intermediates detected (*33*).

Conformational Differences between OASS-A and OASS-B. Spectroscopic signals are sensitive probes of conformational states, reflecting distinct protein flexibility and dynamics that might escape detection by X-ray crystallographic analysis. Absorbance and fluorescence emission spectra of OASS-A and OASS-B, collected under the same experimental conditions, reflect several distinct features.

Polarity of the Active Site and Microenvironment of Tryptophan Residues. It is well established that chromophores and, to a larger extent, fluorophores are good reporters of the polarity of the microenvironment in which they reside. In particular, bathochromic shifts of the absorption bands of aromatic molecules are often observed as a consequence of an increase in the polarity of the microenvironment (*36*). Solvent polarity also affects the emission spectra of aromatic compounds as a consequence of the rearrangement of the solvent molecules around the increased dipole moment of the excited state (*37*). The higher fraction of excitation energy lost in the interaction with polar solvents leads to a red shift of the emission bands. Excitation of tryptophans at 298 nm results in emission peaks centered at ~325 nm when residues are completely buried within the protein core and at ~350 nm when the amino acid is completely exposed to bulk solvent (*38*). The emission band of the tryptophan residues of OASS-B is blue shifted by 2 nm with respect to the emission band of OASS-A (Figure 8A). The structure of the B-isozyme indicates that, while the conserved tryptophans W28 and W159 are at least partially exposed to the solvent, the third one, W212, is deeply buried inside the protein and might be responsible for the slightly blue-shifted emission maximum.

The active site polarity for the ISB intermediate is slightly higher in the B-isozyme compared to the A-isozyme, likely due to the presence of two ionizable residues, D281 and C280, as discussed above. From a spectroscopic point of view the increased polarity of the OASS-B active site is supported by a 2 nm red shift in the absorption band of the ketoenamine tautomer with respect to that of OASS-A (Figure 4A). Also, in the excited state, the coenzyme in OASS-B experiences a more polar environment than in OASS-A, as demonstrated by the red shift from 505 to 511 nm of the ketoenamine emission band upon excitation at 412 nm (Figure 8C).

Conversion to the ESB upon addition of substrate is expected to involve a conformational change that causes, among other things, the exclusion of water molecules from the active site. Formation of the ESB in the B-isozyme is accompanied by a larger bathochromic shift of the ketoenamine tautomer absorption band (13 nm; Figure 4C) with respect to the same species in the A-isozyme (6 nm). This finding suggests a more pronounced increase in the active site microenvironment polarity in the case of OASS-B, likely due to a repositioning of charged or polar residues around the cofactor, consistent with the proposed effect of ionization of C280.

Tautomeric Equilibria and Enzyme Dynamics. ISB, ESB, and AA intermediates can exist as enolimine and ketoenamine tautomeric forms in equilibrium (Scheme 1). It is generally believed that, due to charge separation, the ketoenamine tautomer is stabilized over the enolimine tautomer in polar environments (*13*). In previous studies of PLP model compounds, like the PLP-valine Schiff base (ref *10* and references cited therein), the peak at 420 nm observed upon excitation at 330 nm was attributed to the direct emission of the enolimine tautomer (*10*). Thus, in the fluorescence spectrum of OASS-B (Figure 8), upon excitation at either 298 nm or 330 nm, the band at 425 nm can be attributed to the emission of the enolimine tautomer of the internal aldimine. Upon excitation at 298 nm, tryptophan emission is followed by an energy transfer event from tryptophan(s) to the coenzyme, made possible by the spectral overlap of the tryptophan emission and enolimine absorption bands and by a distance ≤25 Å separating donor and acceptor.

Excitation of the A-isozyme at 298 nm gives an emission spectrum in the visible range with a band centered at 500 nm, while the band centered at 425 nm observed in the spectrum of the B-isozyme is absent. The 500 nm band is

generated by the emission of the ketonamine tautomer (*10*) as a consequence of a complex process (*12*). Upon excitation of the A-isozyme at 298 nm, the energy transfer from tryptophan(s) to the enolimine tautomer is followed by an isomerization in the excited state to give the ketoenamine tautomer, which emits at 500 nm (*10*). The isomerization of the enolimine tautomer in OASS-B does not take place, or if this happens, the process is not as efficient as in OASS-A. Consequently, the emission of the ketoenamine of OASS-B results in only a broadening of the 425 nm band on the red side. Accordingly, the intensity of the emission band in OASS-B that results from direct excitation of the enolimine is increased in intensity by more than 5-fold compared to that in OASS-A (Figure 8B).

The slightly higher population of the enolimine tautomer in the ISB of OASS-B compared to OASS-A (Figure 4A) is reversed once the ESB is formed (Figure 4C). The more polar environment of OASS-B is accompanied by the almost exclusive accumulation of the ketoenamine tautomer of the ESB, as judged by the different peak ratios at 325 and 418/427 nm in the absorbance spectrum. The formation of the ESB intermediate in the presence of L-serine is also characterized by an increase in intensity and a blue shift of the ketoenamine emission band upon excitation at either 298 or 412 nm, for both isozymes and to a greater extent for OASS-B (Figure 9A). In principle, this could be due to an increase in the enolimine tautomer population or to a change in PLP orientation, both of which can affect the degree of energy transfer from tryptophan residues to the cofactor. Structural analysis of the OASS-A external aldimine (*5*) indicated that the coenzyme tilts by 13° along its longitudinal axis in the transition from the internal aldimine to the external aldimine, and this same change is expected for OASS-B. An increase in the lifetime of the Schiff base excited state can also lead to an increase in emission intensity, as previously proposed for OASS-A (*11*). The increase in excited state lifetime is the most likely explanation for the B-isozyme as well, since enhancement of the 500 nm emission band in the presence of serine occurs without affecting the intensity and position of the 336 and 425 nm bands.

The blue shift of the ketoenamine tautomer emission band of the ESB with respect to ISB (Figure 9B) indicates a shielding of the active site from bulk solvent brought about by the conformational change that accompanies the transition from the ISB to the ESB, as also evidenced in structural studies of an OASS-A mutant (*24*).

Striking differences between OASS-A and OASS-B are observed in emission spectra upon excitation at 298 nm in the presence of acetate. Previous studies of OASS-A suggested that binding of acetate resulted in an enhancement of the fluorescence emission at 500 nm with a blue shift of the peak and no effect on the tryptophan emission (*10*, *11*). The spectroscopic changes are a consequence of the abortive occupation of the substrate α-carboxylate subsite by acetate and the subsequent triggering of a partial closure of the active site, as also pointed out for the interaction of the carboxy-terminal peptide of serine acetyltransferase with OASS-A (*14*). As observed for OASS-A (*11*), when acetate binds to the B-isozyme, the tryptophan emission is virtually unaffected. However, acetate binding results in an appearance of the band at 498 nm and the concomitant decrease in the band at 425 nm, suggesting a change in the rate of the isomerization of the enolimine to the ketoenamine tautomer in the excited state. Thus, formation of the external aldimine only affects the quantum yield of the ketoenamine emission, while acetate binding to the α-carboxylate subsite appears to trigger a conformational change that affects the lifetime of the Schiff base fluorescence and also affects the equilibrium between different tautomeric forms of the ISB. Such an effect on tautomer interconversion suggests that the A and B isozymes of OASS might differ not only in the polarity of the active site environment but also in terms of the structural flexibility, i.e., the capability to undergo conformational transitions along the reaction pathway. A difference in flexibility might help to explain the observed differences in the catalytic efficiency of the two isoforms of the enzyme beyond any mechanistic considerations of the effect of the presence or absence of different polar or charged groups in the proximity of PLP. This difference in flexibility seems to be consistent with the higher *B*-factors observed for OASS-B with respect to OASS-A (Figure 2 and Table 2).

CONCLUSIONS

The overall three-dimensional fold of OASS-B is very similar to that of OASS-A. The active site of the B-isozyme, however, differs from that of the A-isozyme in the presence of two additional acidic residues, D241 and C280. The presence of these residues increases the overall charge in the site, which is translated to an increased pK_a for the Schiff base lysine in the AA intermediate. The ionization state of C280 is thought to be responsible for regulating the amount of the ESB formed with serine and cysteine and, by analogy, OAS; K_{ESB} is pH independent over the range 7.5 to >10.0.

The other major difference between the A- and B-isozymes resides in the difference in rates of their overall reactions. The V/E_t with TNB as the nucleophilic substrate is 10-fold greater, and the first-order rate constant for decomposition of the AA is 40-fold greater in the case of the B-isozyme. The reason for this difference is not easily understood. Comparison of the spectrofluorometric properties of the ISB and catalytic intermediates for both OASS-A and OASS-B provides indications of a different equilibrium distribution between enolimine and ketoenamine tautomers and hints of distinct differences in flexibility, as indicated by the detailed analysis of the crystallographic *B*-factors for both isoforms.

REFERENCES

1. Kredich, N. M., and Tomkins, G. M. (1966) The enzymic synthesis of L-cysteine in *Escherichia coli* and *Salmonella typhimurium*, *J. Biol. Chem. 241*, 4955−4965.
2. Tai, C. H., Nalabolu, S. R., Jacobson, T. M., Minter, D. E., and Cook, P. F. (1993) Kinetic mechanisms of the A and B isozymes of *O*-acetylserine sulfhydrylase from *Salmonella typhimurium* LT-2 using the natural and alternative reactants, *Biochemistry 32*, 6433−6442.
3. Tai, C. H., Nalabolu, S. R., Simmons, J. W., III, Jacobson, T. M., and Cook, P. F. (1995) Acid-base chemical mechanism of *O*-acetylserine sulfhydrylases-A and -B from pH studies, *Biochemistry 34*, 12311−12322.
4. Burkhard, P., Rao, G. S., Hohenester, E., Schnackerz, K. D., Cook, P. F., and Jansonius, J. N. (1998) Three-dimensional structure of *O*-acetylserine sulfhydrylase from *Salmonella typhimurium*, *J. Mol. Biol. 283*, 121−133.
5. Burkhard, P., Tai, C. H., Ristroph, C. M., Cook, P. F., and Jansonius, J. N. (1999) Ligand binding induces a large confor-

mational change in *O*-acetylserine sulfhydrylase from *Salmonella typhimurium*, *J. Mol. Biol. 291*, 941−953.
6. Burkhard, P., Tai, C. H., Jansonius, J. N., and Cook, P. F. (2000) Identification of an allosteric anion-binding site on *O*-acetylserine sulfhydrylase: structure of the enzyme with chloride bound, *J. Mol. Biol. 303*, 279−286.
7. Claus, M. T., Zocher, G. E., Maier, T. H., and Schulz, G. E. (2005) Structure of the *O*-acetylserine sulfhydrylase isoenzyme CysM from *Escherichia coli*, *Biochemistry 44*, 8620−8626.
8. Benci, S., Bettati, S., Vaccari, S., Schianchi, G., Mozzarelli, A., and Cook, P. F. (1999) Conformational probes of *O*-acetylserine sulfhydrylase: fluorescence of tryptophans 50 and 161, *J. Photochem. Photobiol. B 48*, 17−26.
9. Benci, S., Vaccari, S., Mozzarelli, A., and Cook, P. F. (1997) Time-resolved fluorescence of *O*-acetylserine sulfhydrylase catalytic intermediates, *Biochemistry 36*, 15419−15427.
10. Benci, S., Vaccari, S., Mozzarelli, A., and Cook, P. F. (1999) Time-resolved fluorescence of *O*-acetylserine sulfhydrylase, *Biochim. Biophys. Acta 1429*, 317−330.
11. McClure, G. D., Jr., and Cook, P. F. (1994) Product binding to the alpha-carboxyl subsite results in a conformational change at the active site of *O*-acetylserine sulfhydrylase-A: evidence from fluorescence spectroscopy, *Biochemistry 33*, 1674−1683.
12. Strambini, G. B., Cioni, P., and Cook, P. F. (1996) Tryptophan luminescence as a probe of enzyme conformation along the *O*-acetylserine sulfhydrylase reaction pathway, *Biochemistry 35*, 8392−8400.
13. Faeder, E. J., and Hammes, G. G. (1970) Kinetic studies of tryptophan synthetase. Interaction of substrates with the B subunit, *Biochemistry 9*, 4043−4049.
14. Campanini, B., Speroni, F., Salsi, E., Cook, P. F., Roderick, S. L., Huang, B., Bettati, S., and Mozzarelli, A. (2005) Interaction of serine acetyltransferase with *O*-acetylserine sulfhydrylase active site: evidence from fluorescence spectroscopy, *Protein Sci. 14*, 2115−2124.
15. Monroe, R. S., and Kredich, N. M. (1988) Isolation of *Salmonella typhimurium cys* genes by transduction with a library of recombinant plasmids packaged in bacteriophage P22HT capsids, *J. Bacteriol. 170*, 42−47.
16. Becker, M. A., Kredich, N. M., and Tomkins, G. M. (1969) The purification and characterization of *O*-acetylserine sulfhydrylase-A from *Salmonella typhimurium*, *J. Biol. Chem. 244*, 2418−2427.
17. Peterson, E. A., and Sober, H. A. (1954) Preparation of crystalline phosphorylated derivatives of vitamin B6, *J. Am. Chem. Soc. 76*, 169−175.
18. Otwinowski, Z., and Minor, W. (1997) Processing of X-ray diffraction data collected in oscillation mode, in *Methods in Enzymology* (Charles W. Carter, J., Ed.) Part A, pp 307−326, Academic Press, San Diego.
19. Kantardjieff, K. A., and Rupp, B. (2003) Matthews coefficient probabilities: Improved estimates for unit cell contents of proteins, DNA, and protein-nucleic acid complex crystals, *Protein Sci. 12*, 1865−1871.
20. Navaza, J. (1994) AMoRE—an automated package for molecular replacement, *Acta Crystallogr. A 50*, 157−163.
21. Jones, T. A., Zou, J. Y., Cowan, S. W., and Kjeldgaard, M. (1991) Improved methods for building protein models in electron-density maps and the location of errors in these models, *Acta Crystallogr. A 47*, 110−119.
22. Brunger, A. T., Adams, P. D., Clore, G. M., DeLano, W. L., Gros, P., Grosse-Kunstleve, R. W., Jiang, J. S., Kuszewski, J., Nilges, M., Pannu, N. S., Read, R. J., Rice, L. M., Simonson, T., and Warren, G. L. (1998) Crystallography & NMR system: A new software suite for macromolecular structure determination, *Acta Crysallogr. D 54*, 905−921.
23. Collaborative Computational Project, Number 4 (1994) The CCP4 suite: programs for protein crystallography, *Acta Crystallogr. D 50*, 760−763.
24. Schnackerz, K. D., Tai, C. H., Simmons, J. W., III, Jacobson, T. M., Rao, G. S., and Cook, P. F. (1995) Identification and spectral characterization of the external aldimine of the *O*-acetylserine sulfhydrylase reaction, *Biochemistry 34*, 12152−12160.
25. Cook, P. F., Hara, S., Nalabolu, S., and Schnackerz, K. D. (1992) pH dependence of the absorbance and ^{31}P NMR spectra of *O*-acetylserine sulfhydrylase in the absence and presence of *O*-acetyl-L-serine, *Biochemistry 31*, 2298−2303.
26. McLachlan, A. (1982) Rapid comparison of protein structures, in *Acta Crystallogr. A*, 871−873.
27. Laskowski, R. A., Macarthur, M. W., Moss, D. S., and Thornton, J. M. (1993) PROCHECK—a program to check the stereochemical quality of protein structures, *J. Appl. Crystallogr. 26*, 283−291.
28. Tai, C. H., Burkhard, P., Gani, D., Jenn, T., Johnson, C., and Cook, P. F. (2001) Characterization of the allosteric anion-binding site of *O*-acetylserine sulfhydrylase, *Biochemistry 40*, 7446−7452.
29. Cook, P. F., and Wedding, R. T. (1976) A reaction mechanism from steady-state kinetic studies for *O*-acetylserine sulfhydrylase from *Salmonella typhimurium* LT-2, *J. Biol. Chem. 251*, 2023−2029.
30. Goldberg, M. E., York, S., and Stryer, L. (1968) Fluorescence studies of substrate and subunit interactions of the beta-2 protein of *Escherichia coli* tryptophan synthetase, *Biochemistry 7*, 3662−3667.
31. Daum, S., Tai, C. H., and Cook, P. F. (2003) Characterization of the S272A,D site-directed mutations of *O*-acetylserine sulfhydrylase: involvement of the pyridine ring in the alpha,beta-elimination reaction, *Biochemistry 42*, 106−113.
32. Flint, D. H., Tuminello, J. F., and Miller, T. J. (1996) Studies on the synthesis of the Fe-S cluster of dihydroxy-acid dehydratase in *Escherichia coli* crude extract. Isolation of *O*-acetylserine sulfhydrylases A and B and beta-cystathionase based on their ability to mobilize sulfur from cysteine and to participate in Fe-S cluster synthesis, *J. Biol. Chem. 271*, 16053−16067.
33. Hwang, C. C., Woehl, E. U., Minter, D. E., Dunn, M. F., and Cook, P. F. (1996) Kinetic isotope effects as a probe of the beta-elimination reaction catalyzed by *O*-acetylserine sulfhydrylase, *Biochemistry 35*, 6358−6365.
34. Cook, P. F., Tai, C. H., Hwang, C. C., Woehl, E. U., Dunn, M. F., and Schnackerz, K. D. (1996) Substitution of pyridoxal 5′-phosphate in the *O*-acetylserine sulfhydrylase from *Salmonella typhimurium* by cofactor analogs provides a test of the mechanism proposed for formation of the alpha-aminoacrylate intermediate, *J. Biol. Chem. 271*, 25842−25849.
35. Rabeh, W. M., and Cook, P. F. (2004) Structure and mechanism of *O*-acetylserine sulfhydrylase, *J. Biol. Chem. 279*, 26803−26806.
36. Bergethon, P. R. (1998) *The Physical Basis of Biochemistry: The Foundations of Molecular Biophysics*, Springer-Verlag, New York.
37. Lakowicz, J. R. (1983) *Principles of Fluorescence Spectroscopy*, Plenum Press, New York.
38. Burstein, E. A., Vedenkina, N. S., and Ivkova, M. N. (1973) Fluorescence and the location of tryptophan residues in protein molecules, *Photochem. Photobiol. 18*, 263−279.

BI602603C